Journal of Rock Mechanics and Geotechnical Engineering 11 (2019) 1184–1200

Contents lists available at ScienceDirect

Journal of Rock Mechanics and Geotechnical Engineering

journal homepage: www.rockgeotech.org

Full Length Article

Numerical investigations of rock bridge effect on open pit slope stability

C. Romer [a], M. Ferentinou [b,*]

[a] Geological Sciences, University of KwaZulu Natal, Durban, South Africa
[b] Civil Engineering Science, University of Johannesburg, Johannesburg, South Africa

ARTICLE INFO

Article history:
Received 3 August 2018
Received in revised form
29 December 2018
Accepted 7 March 2019
Available online 17 October 2019

Keywords:
Ubiquitous model
Veneziano model
Parallel deterministic joint network
Numerical modelling
Rock slope stability
Discontinuities
Open pit

ABSTRACT

In this study, the effect of rock bridges on rock slope stability was investigated by incorporating non-persistent joint networks in numerical models, and the critical profiles of an open pit mine were analysed. Parallel deterministic networks of infinite and finite lengths, ubiquitous joint network model and Veneziano joint network model were used in order to simulate the rock fractures. Materials were modelled based on the generalised Hoek–Brown and equivalent Mohr–Coulomb failure criteria. The parallel deterministic infinite and the ubiquitous joint network models produced lower safety factors. The introduction of rock bridges along discontinuity planes in the parallel deterministic network and Veneziano joint network models significantly contributed to the stability and strain distribution, which should be considered in stability analysis of rock mass in open pit by rock slope practitioners. The results show the significance of joints in hard rock behaviour and the joints should be included in order to attain practical and realistic simulations.

1. Introduction

Rock bridges are recognised as a critical factor in the stability of rock slopes. However, they still remain a challenging problem with respect to their measurement and incorporation into design analysis (Elmo et al., 2018). It remains problematic that their presence prior to failure is not visible unless the rock mass is exposed. Therefore, in order to accommodate them in a rock slope stability analysis, engineering practitioners generally rely on structural geological measurements. It is promising that new methods to quantify discontinuity persistence are developed based on remote sensing techniques (Tuckey and Stead, 2016; Riquelme et al., 2018).

In rock slope stability analysis, the failure mechanism is often assumed to be associated with the sliding of rock blocks along pre-existing discontinuities. In addition to instability resulting from the existing discontinuity surfaces themselves, all the induced fracture surfaces could interact through complex mechanisms to facilitate the formation of significant shear or tensile failure surfaces (Stacey et al., 2003; Eberhardt et al., 2004).

On the contrary, when non-persistent joints are presented, the definition and distribution of damage are strongly related to the presence of rock bridges (Stead and Eberhardt, 2013). Tuckey and Stead (2016) also suggested that because of the difference in the shear strengths (defined by the cohesion and frictional components) of the intact rock and natural discontinuities, the existence of relatively small intact rock bridges reduces the development of potential damage and increases the stability of a rock slope.

Although the importance of intact rock bridges for slope stability has been widely recognised and qualitatively understood for decades, there are still no mature methods for estimating the intact rock content of a rock slope and incorporating intact rock bridges into slope stability analysis (Tuckey and Stead, 2016).

Over the last decades, advance in computer power and numerical modelling algorithms allowed for the development of sophisticated methods for analysis of complex rock slope failures, including explicit discontinuities, fracture propagation and coalescence. Popular methods used include extended finite element method (XFEM) (Belytscho and Black, 1999; Moes et al., 1999), explicit distinct element method (DEM) such as the universal distinct element code UDEC (Cundall and Strack, 1979), implicit DEM such as discontinuous deformation analysis (DDA) (Shi and Goodman, 1985), particle flow code (PFC) (Itasca, 2011), methods based on the finite element mesh (e.g. FRANC) or coupling with the DEM (e.g. ELFEN), conventional finite element method (FEM) (Eberhardt et al., 2004; Stead et al., 2006), numerical manifold

* Corresponding author.
E-mail address: mferentinou@uj.ac.za (M. Ferentinou).
Peer review under responsibility of Institute of Rock and Soil Mechanics, Chinese Academy of Sciences.

https://doi.org/10.1016/j.jrmge.2019.03.006

method (NMM) (Shi, 1991, 1992), and coupling method (e.g. FEM/DDA) which is capable of dealing with both continuous and discontinuous problems.

In this context, we propose a typical approach for modelling hard rocks with natural discontinuities, from data collection based on field measurements to numerical simulation using commercially available code where geotechnical engineering practitioners usually have access. Two-dimensional (2D) stochastic fracture traces are embedded in FDEM or FEM models to simulate the effect of persistence on rock slope stability. The aim is to understand the effect of rock bridge inclusion in rock slope stability analysis, whereas neglecting the persistence of structural discontinuities may lead to oversimplification and an unrealistic prediction of failure mechanism and safety factor.

2. Discontinuity persistence in slope stability and joint network models

2.1. Discontinuity persistence

Terzaghi (1962), Jennings (1970) and Einstein et al. (1983) suggested that slope failure results from complex interaction between existing natural discontinuities and brittle fracture propagation through intact rock bridges, and they recognised the importance of potential "step-path" rock slope failures. Wong and Wu (2014) explained that massive rock slope instability inherently requires the evolution of natural discontinuities through a gradual discontinuous–continuous transition to fully discontinuous medium, and they simulated progressive step-path failure of rock slopes.

Persistence can be defined as the continuous length of a discontinuity within a single plane and it delineates the block size as well as the length of potential failure surfaces (Hoek and Bray, 1981). According to Einstein et al. (1983), discontinuities with a persistence which allows for small rock bridges can substantially increase rock mass strength. Rock bridges refer to as the gaps of intact material between disrupted joint planes (Terzaghi, 1962). The shear strength of discontinuities and its controlling factors are important in the analysis of structurally dominated rock slopes since discontinuity surface roughness increases its shear strength and could play partial role in stabilising rock slope (Hoek, 2007).

Hoek and Bray (1981) suggested that the spacing of discontinuities is important as it defines the dimensions of blocks and thus the size of a potentially unstable block. The dimensions are calculated using the spacing and number of sets as well as the persistence, whereas the block shapes are determined using only the number of sets and their orientations (Zhang, 2016). Rock mass strength can also be assessed through discontinuity intensity where highly fractured media tend to form a continuous weak zone due to the merging of multiple closely spaced discontinuities (Hoek and Bray, 1981).

2.2. Joint network models

Joints in a rock mass are often required to be defined integrally rather than individually, as previously recognised, basically due to the difficulties in describing their exact geometric and mechanical properties such as partial visibility of an entire joint plane and inaccessible areas for direct observation (Dershowitz and Einstein, 1988). Numerous methods have been developed to deal with uncertainty related to the geometric properties of joint networks (Jimenez-Rodriguez and Sitar, 2008). Dershowitz and Einstein (1988) described several stochastic joint models where an assemblage of joints is described by an approach known as aggregate characterisation. Some of the models employed to symbolise rock mass geometry and to quantify the spatial variability of joint geometry include the ubiquitous, parallel deterministic and Veneziano joint network models. These joint networks are employed in order to observe the behaviour of rock masses with the application of critical joint sets. These models can capture the interdependence of several characteristics and thus describe the rock mass geometry as an entity which is more complete representation of reality (Dershowitz and Einstein, 1988).

The ubiquitous joint model introduces joints into originally isotropic intact rock to form a jointed rock mass where anisotropy of joint strength and deformability is presented in order that the rock mass remains isotropic (Wang and Huang, 2009). Directional variation of rock properties, or anisotropy, is typically associated with distinct fabric elements in the form of bedding, foliation in metamorphic rocks or intense jointing (Amadei et al., 1987). According to Jakubec et al. (2001), the ubiquitous joint model can be used for failure simulations and is defined as an anisotropic plasticity model that exhibits strength anisotropy in a series of weak planes with predefined joint parameters. In the ubiquitous joint model, the specific parameters include joint direction and shear strength properties, whereas other physical properties that are not defined include joint spacing and location (Valdivia and Lorig, 2001). The geomechanical properties of the material and joints determine the failure occurrence through the solid material itself, or along a weak plane, or both (Singh et al., 1994; Soren et al., 2014). According to Amadei et al. (1987), during mining operations, the principal stress aligns with the dip direction of ubiquitous joints (Fig. 1). This stress adjustment encourages movement along these joints and may lengthen them (Call et al., 2001), thereby increasing potential slip surfaces and ultimately the magnitude of slope failures. The ubiquitous joint model has been used by several authors to account for the presence of weak planes (e.g. Jakubec et al., 2001; Sjöberg, 2001; Valdivia and Lorig, 2001; Li et al., 2003).

The parallel deterministic joint model (Fig. 2a and b) simulates a network of several parallel joints having a constant orientation, spacing and persistence, allowing for randomisation of the location of joints (Wen et al., 2014; Moradi and Hosseinitoudeshki, 2015).

The Veneziano model was developed by Veneziano (1978) to represent the trace planes in two or three dimensions. This model is based on the Poisson plane and Poisson line process (Dershowitz and Einstein, 1988). A system of joints represented by Poisson lines has been found to resemble joint networks in numerous geologies (Dershowitz and Einstein, 1988). The Poisson line process assumes the infinite extent of joints, thus introducing problems into simulating unbounded joints. This is the reason that Veneziano (1978) adopted this concept in modelling of bounded joints. The improved model is created through three random processes, the

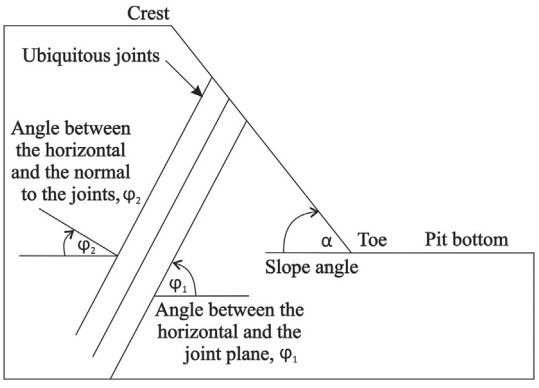

Fig. 1. 2D ubiquitous joint model (modified from Sjöberg, 1999).

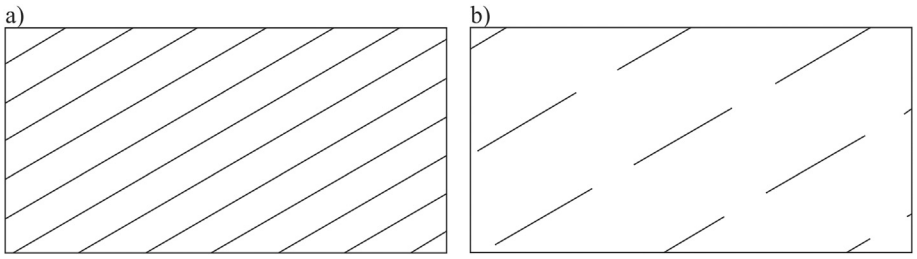

Fig. 2. Parallel deterministic joint network with (a) joints of infinite length and (b) non-persistent joints.

first being the generation of joint planes as Poisson planes with a specified distribution of orientation (Fig. 3a). The Poisson line process on each joint plane subsequently divides joint planes into numerous polygons which represent joint shapes (Fig. 3b). The third and final steps involve random selection of a portion of these polygons, which are selected based on persistence, to be defined as being jointed and the remaining portion as intact rock (Fig. 3c). This model defines joint size according to the intensity of both the Poisson line process and the amount of 'joint' polygons (Dershowitz and Einstein, 1988). The use of joint planes tends towards coplanar jointing and in 2D trace planes, which are represented by coplanar segments or fibres (Fig. 3d).

3. Materials and methods

Slope stability analyses were conducted based on three representative critical profiles selected from structural domains of known concern in terms of problematic design domains and pertaining to reports by Consultant A (1996), Consultant B (2006), Consultant C (2009) and Consultant D (2011) (Fig. 4). The geotechnical model comprising the geological, structural and rock mass models of these profiles was found to vary in complexity in terms of the number of materials it comprises, where profile *B* consists of a single material as opposed to profiles *A* and *C* having multiple materials (Fig. 4).

3.1. Strength properties of intact rock

All material types were considered to be isotropic, having identical mechanical properties in all directions, thus behaving uniformly when subjected to stress. All materials were specified to be plastic in nature in order that their strength properties can be employed in the analysis of stresses and displacements in the event of failure. Furthermore, identical peak and residual strength properties (tensile strength, friction angle and cohesion) were used so as

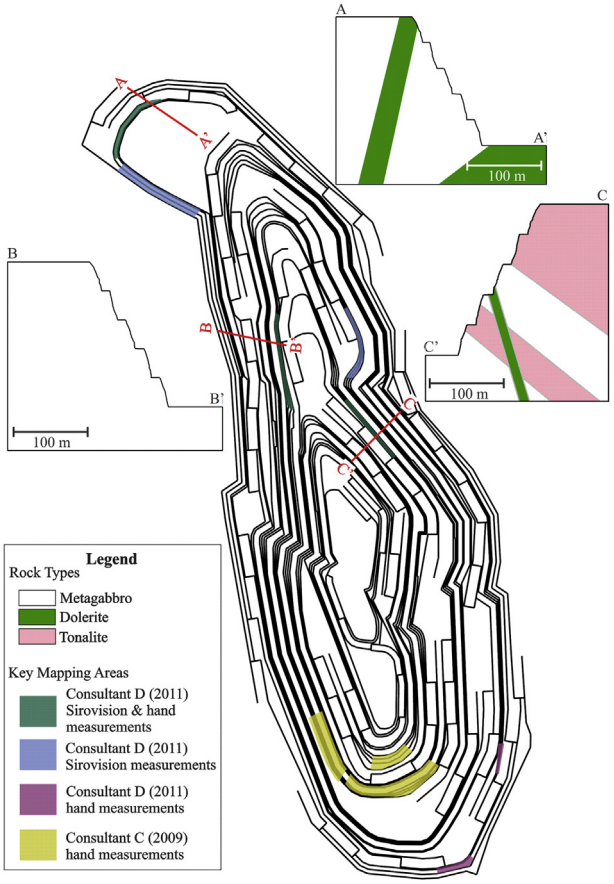

Fig. 4. Pit configuration and measurement zones from consultants with critical profiles' locations.

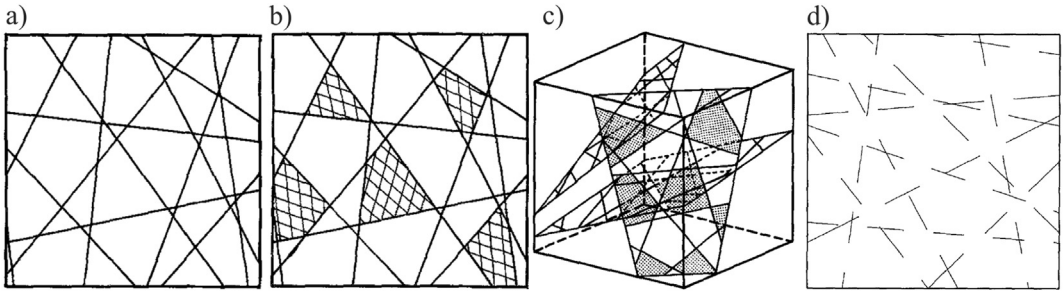

Fig. 3. Generation of the Veneziano joint system model: (a) 2D Poisson line process; (b) Marking of polygonal joints; (c) Three-dimensional (3D) Poisson plane process; and (d) 2D Veneziano model where joints are represented as coplanar segments (Dershowitz and Einstein, 1988).

Table 1
Typical properties of varying rock mass quality (Hoek and Brown, 1997).

Rock mass quality	σ_{ci} (MPa)	m_i	GSI	ϕ' (°)	c' (MPa)	σ_{cm} (MPa)	σ_{tm} (MPa)	E_m (GPa)	ν
Very good	150	25	75	46	13	64.8	−0.9	42	0.2
Average	80	12	55	33	3.5	13	−0.15	9	0.25
Very poor	20	8	30	24	0.55	1.7	−0.01	1.4	0.3

Table 2
Rock mass strength properties.

Hoek–Brown classification						Hoek–Brown criterion		
Soil	σ_{ci} (MPa)	GSI	m_i	D	m_b	m_b	s	a
Metagabbro	299.15	70	11.07	1	1.3	1.3	0.0067	0.5
Tonalite	214.05	67	33.6	1	3.18	3.18	0.0041	0.5
Dolerite	145	62	16	1	1.06	1.06	0.0018	0.5

Failure envelope range				Mohr–Coulomb fit		Rock mass parameters		
Application	σ_{3max} (MPa)	γ (MN/m^3)	Slope height (m)	c (MPa)	ϕ (°)	σ_t (MPa)	σ_c (MPa)	σ_{cm} (MPa)
Slopes	4.82	0.028	200	4.24	49.19	−1.55	24.39	48.47
	4.84	0.028	200	2.84	55.23	−0.27	13.56	51.54
	4.45	0.028	200	1.73	44	−0.24	6.02	20.16

to define an elastic-perfectly plastic material where the rock mass continues to deform while keeping its strength and not changing its volume (Hoek and Brown, 1997). The use of a disturbance factor of $D = 0.7$ or higher results in post-failure strength and modulus reduction, thus it makes this model viable when better quality hard rock masses are experienced (Hoek, 2007). Solutions from elastic-perfectly plastic stress–strain relations can be proportional to those of the conventional limit equilibrium methods (LEMs) which are the most commonly used model in calculation of safety factors in the FEM (Zheng et al., 2005). The elastic properties were defined by the Young's modulus (E_m) and Poisson's ratio (ν). Due to the limited data, estimates of these parameters were based upon typical values from practical problems addressed by Hoek and Brown (1997). Values of 42 GPa and 0.2 for E_m and ν were assumed in this study, respectively. Selection of these values was related to the geological strength index (GSI) of 67, 70 and 62 for hard rocks of tonalite, metagabbro and dolerite, respectively, which were calculated by Consultant B (2006). These values correspond to the 'very good quality' hard rock mass category defined by Hoek and Brown (1997) (see Table 1).

The strength of jointed rock masses was estimated using the generalised Hoek–Brown strength criterion (Hoek and Brown, 1980) which relied upon the uniaxial compressive strength (UCS, σ_{ci}) values (Consultant B, 2006), m_i constant of intact rock, GSI and disturbance factor D (Consultant C, 2009). The triaxial test results were imported into RocData 5.0 (Rocscience Inc., 2015) to obtain representative and reliable estimates of rock mass strength parameters related to the generalised Hoek–Brown strength criterion (Hoek et al., 2002) and equivalent Mohr–Coulomb strength criterion. The minor and major principal stresses (σ_3 and σ_1, respectively) values resulted in UCS (σ_{ci}) values of 299.15 MPa and 214.05 MPa and m_i constant values of 11.07 and 33.6 for metagabbro and tonalite, respectively (Table 2). A value of $D = 1$, as suggested by Consultant B (2006), was used and corresponded to a 'disturbed' rock mass which may be attributed to blast damage and stress relief from overburden rock removal (Hoek and Brown, 1988). These parameters were derived by performing a curve fit of laboratory data using the modified cuckoo fitting algorithm (Walton et al., 2011). This algorithm is used in the calculation of residuals or errors which give an indication of how well the selected strength criterion fits the triaxial test data set. The resulting residuals for metagabbro and tonalite were 52,295 and 24,242, respectively. Based on the input values of σ_{ci}, GSI, m_i and D, the strength properties of Hoek–Brown criterion, m_b, s and a, were computed (Table 2). The parameters of the equivalent Mohr–Coulomb criterion, cohesion (c) and friction angle (ϕ), were calculated simultaneously (Table 2). The resulting rock mass properties were employed in the numerical analyses.

The GSI values were estimated directly from the rock mass rating (RMR) (Bieniawski, 1989; Consultant B, 2006). The Mohr–Coulomb best-fit envelope was generated in RocData (Rocscience Inc., 2015) based on a defined stress range which was in turn dependent on the field of application. In this case, slopes with a height of 200 m and an average material unit weight, γ, of 0.028 MN/m^3 (Table 2) were analysed. Rock mass parameters were also calculated, including the tensile strength (σ_t), UCS (σ_c) and the global strength (σ_{cm}) (Table 2). The principal stress (σ_1 vs. σ_3) and the shear-normal stress (τ vs. σ_n) failure envelopes were plotted automatically in order to observe the effects of strength parameters on the shape of failure envelopes (Fig. 5).

3.2. Shear strength of discontinuities

Input data related to the shear strength of failure surfaces include selection of preferred joint shear strength model and associated properties. In this study, the Mohr–Coulomb shear strength model or slip criterion was employed with the friction angle (ϕ_{joint}) and cohesion (c_{joint}) being used as the inputs.

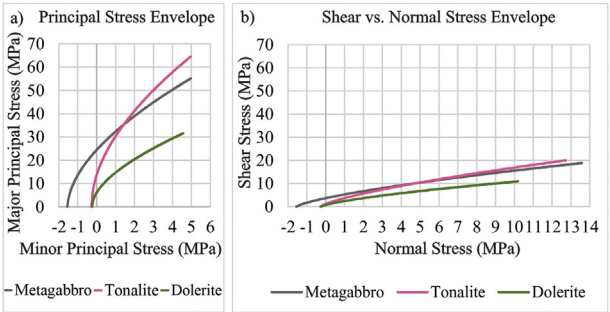

Fig. 5. Principal stress and shear-normal failure envelopes for metagabbro, tonalite and dolerite.

Consultant C (2009) determined the basic friction angles (ϕ_b) of metagabbro and dolerite by performing shear tests on saw-cut samples. Instantaneous friction (ϕ_i) and cohesion values were determined using the Barton–Bandis equation (Barton, 1973, 1976) which relies on normal statistical distributions for joint roughness coefficient (JRC) (based on typical roughness profiles) and basic friction angles (ϕ_b) as well as average values of joint compressive strength (JCS), normal stress (σ_n) and unit weight (γ). The average of the combined data was subsequently used in the Monte Carlo simulation risk analysis programme @Risk (Palisade, 1997) to obtain statistical ranges of friction and cohesion values. The resulting mean friction angle of 48.82° and cohesion of 0.0145 MPa were used for all discontinuities in this study. The only specified driving force acting on the slope includes gravity. The effect of water pressure on stability was not considered in this study since data related to groundwater conditions were also unavailable, hence all models were assumed to be dry, and the majority of discontinuities in the pit were dry.

Micro- and macro-scale roughness characteristics were estimated for all joints across the pit shell by Consultant D (2011). Micro-scale roughness characteristics were considered to be of a sample length of 200 mm from which JRC was determined using typical joint profiles as prescribed by Barton (1987). Macro-scale roughness in contrast was estimated on a scale of approximately 3–10 m.

The micro-scale roughness of most discontinuities in profiles *A*, *B* and *C* is undulating rough, undulating smooth and undulating smooth again, respectively (Fig. 6a). The macro-scale roughness of most discontinuities in profiles *A*, *B* and *C* is planar, undulating and planar, respectively (Fig. 6b). The type of infilling material within a discontinuity can also have an impact on slope stability by influencing the shear strength of discontinuities. According to Fig. 7, most discontinuities in profiles *A*, *B* and *C* have no infilling materials, and only 15, 30 and 14 discontinuities in profiles *A*, *B* and *C* have calcite as the infilling material, respectively. It should be noted that the majority of data have no information on the infilling type (Sirovision data) or information recorded during field investigations.

The discontinuity persistence of the two main critical joint sets associated with profiles *A*, *B* and *C* is shown in Fig. 8. In joint set 1 of profile *A*, most discontinuities have a persistence ranging between 10 m and 20 m, with a mean of 10 m, a relative minimum of 9.5 m and a relative maximum of 10 m. The same relationship is apparent for joint set 3. In joint set 1 of profile *B*, most discontinuities have a persistence ranging from 3 m to 10 m, resulting in a mean value of 6.5 m and relative minimum and maximum values of 3.5 m. The majority of joints in joint set 2 have a persistence ranging from 1 m to 10 m, resulting in a mean value of 4.5 m, a relative minimum

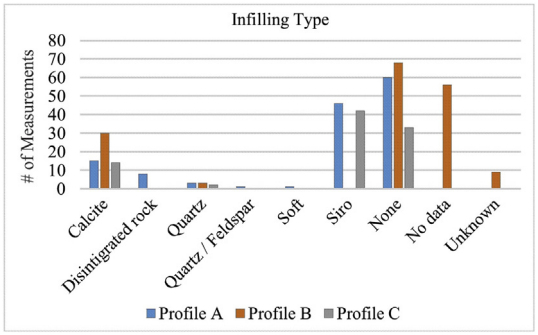

Fig. 7. Discontinuity infilling material for profiles *A*, *B* and *C*.

value of 3.5 m and a relative maximum value of 5.5 m (Fig. 8). Discontinuities of joint set 1 in profile *C* have a persistence ranging from 3 m to 10 m, giving a mean value of 6.5 m and relative minimum and maximum values of 3.5 m, respectively. For set 2, however, the persistence of most discontinuities ranges from 1 m to 3 m, with a mean persistence of 2 m and relative minimum value of 1 m (Fig. 8). These values were employed as inputs of the joint network models.

3.3. Joint network models

Site characterisation uncertainties regarding joints can result in failure to designate specific joints to numerical models. Not surprisingly, true persistence is still considered difficult to be measured in practice (Shang et al., 2017). Therefore, actual persistence seems to be impossible to be measured using the data acquired from the surface. In view of structural data uncertainty, joints were instead incorporated into these models in the form of joint network models in the FEM and ubiquitous joints in the finite difference method (FDM).

The parallel deterministic joint network in Phase2 (Rocscience Inc., 2015) defines discontinuities as a network of parallel joints where the spacing, orientation and length are assumed to be constant. The joint orientations are based on unstable joint sets found in the kinematic analysis (Romer, 2017), where only those responsible for planar and wedge failures are incorporated into the numerical models. The 2D joint spacing was taken to be 5 m and the initial location of the joint network was generated randomly. Results were reported as discontinuities of infinite and finite lengths. Joints of infinite length extended continuously across profiles whereas those of finite length employed the length and persistence as detailed in Table 3, thereby introducing rock bridges into the models. The joint persistence in the model refers to the length of

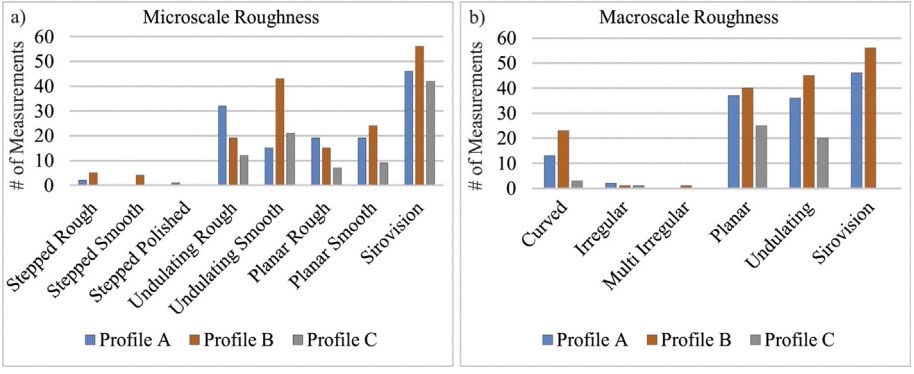

Fig. 6. Micro- and macro-scale roughness of discontinuities.

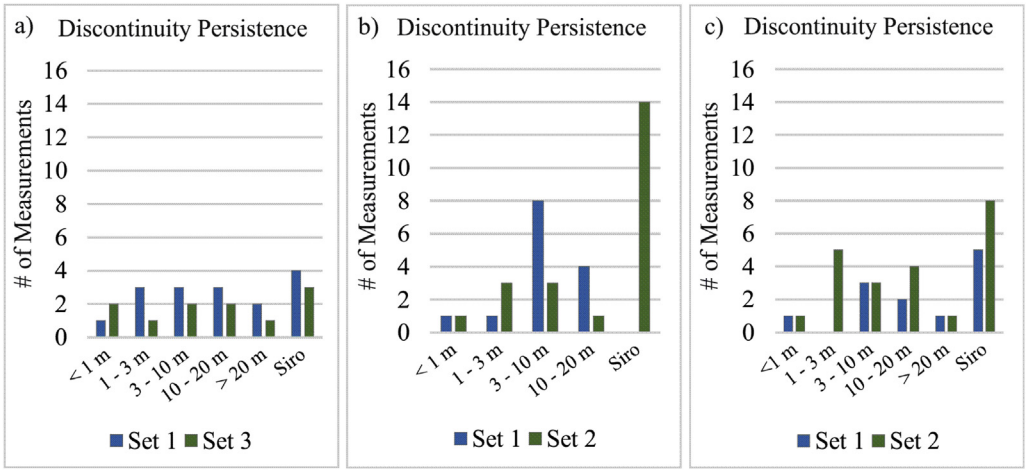

Fig. 8. Discontinuity persistence of critical main joint sets for (a) profile *A*, (b) profile *B* and (c) profile *C*.

Table 3
Joint network properties employed in numerical modelling.

Property	Profile *A*		Profile *B*		Profile *C*	
	J1	J2	J1	J2	J1	J2
Orientation definition						
Joint method	Fisher	Fisher	Fisher	Fisher	Fisher	Fisher
Trace plane dip direction (°)	0	0	0	0	0	0
Mean dip (°)	81	57	56	44	53	87
Mean dip direction (°)	31	128	10	70	298	9
Fisher *K*	5	5	5	5	5	5
Joint length						
Mean	10	10	6.5	4.5	6.5	2
Distribution	Exponential	Exponential	Exponential	Exponential	Exponential	Exponential
Relative minimum (m)	9.5	9.5	3.5	3.5	3.5	1
Relative maximum (m)	10	10	3.5	5.5	3.5	1
Length persistence						
Mean	0.5	0.5	0.5	0.5	0.5	0.5
Distribution	Exponential	Exponential	Exponential	Exponential	Exponential	Exponential
Relative minimum	0.3	0.3	0.3	0.3	0.3	0.3
Relative maximum	0.3	0.3	0.3	0.3	0.3	0.3
Joint intensity measure						
Intensity type	P4	P4	P4	P4	P4	P4
Value	0.5	0.5	0.5	0.5	0.5	0.5
Joint end condition						
Joint ends	Open at boundary contacts	Open at boundary contacts	Open at boundary contacts	Open at boundary contacts	Open at boundary contacts	Open at boundary contacts
Open at surface contact	Yes	Yes	Yes	Yes	Yes	Yes
Open at excavation contact	Yes	Yes	Yes	Yes	Yes	Yes
Property	Profile *A*		Profile *B*		Profile *C*	
	J1	J3	J1	J2	J1	J3
Persistence	0.8	0.8	0.8	0.8	0.8	0.8
Trace plane	No	No	No	No	No	No
Inclination	−81	−57	−56	−44	53	87

intact material, or a rock bridge, between each joint segment. The persistence was defined as 0.8 (Table 3), thus defining approximately 80% of joint continuity and making it comparable to the ubiquitous joint network employed in FLAC (Itasca, 2011). The length values employed were based on mean values of pre-determined discontinuity persistence (Fig. 8a–c). The joint end conditions were specified to be open at the external boundaries in order that two opposite joint faces freely slip relative to one another at exposed faces (Hammah et al., 2009).

The Veneziano joint network was employed to introduce more random and thus more realistic joint conditions since it is based on the Poisson line process (Dershowitz, 1985) which defines random locations of joints and assumes that the joints pass through each of these locations. Joint lengths were defined as random variables based on an exponential distribution where the distribution parameters were again based on the pre-determined discontinuity mean, relative minimum and maximum values of each profile (Table 3). The length persistence was defined as a random variable

Table 4
Discontinuity set measurements for critical profiles.

Profile	Joint set	Mean dip (°)	Mean dip direction (°)	Window dip range (°)	Window dip direction range (°)	Slope face dip direction (°)
A	J1	81	31	66–90, 90–82	44–18, 198–224	133
	J2	83	305	64–90, 90–80	321–284, 104–140	133
	J3	58	128	41–72	116–140	133
B	J1	56	10	41–70	31–347	81
	J2	44	70	32–61	114–37	81
	J3	85	284	71–90, 90–78	294–264, 84–114	81
	J4	85	52	74–90, 90–83	84–20, 200–264	81
	J5	69	235	58–82	210–260	81
C	J1	53	298	42–62	270–329	230
	J2	87	9	74–90, 90–76	31–346, 166–211	230
	J3	6	296	0–15	15–206	230

of exponential distribution having a mean value of 0.5 and relative minimum and maximum values of 0.3 (Table 3). The degree of jointing, known as the joint intensity, was measured as the sum of squared joint trace lengths per unit area. The code associated with the dimensionless measurements is P4 (Table 3). The Fisher *K* value (Fisher, 1953) is a measure of the density of a cluster of orientation data where a larger *K* value suggests a confinement of data in a smaller area as opposed to a *K* value of zero which implies a uniform distribution across the stereonet (Fisher, 1953). A default Fisher *K* value of 5 was used for all joint sets (Table 3).

A plasticity model in FLAC (Itasca, 2011) known as the ubiquitous joint model was used to represent joints in the FDM. The strength properties of the intact material and discontinuities were those associated with the Mohr–Coulomb failure and slip criterion, i.e. the friction angle and cohesion. The joint angles employed include the mean sets determined to be the cause of potential planar and wedge instability in the kinematic analysis. The joint angles added to the models were applied anticlockwise from the *x*-axis.

It is acknowledged that the quantity and quality of data forming a geotechnical model can have major impacts on slope stability analysis results (Fillion and Hadjigeorgiou, 2016). Parameter uncertainty is thus an important consideration in this study since statistical ranges of strength properties are estimated based on the values obtained from imprecise transformation of intact to rock mass parameters.

3.4. Kinematic analysis

Geological orientation data were analysed using dips (Rocscience Inc., 2015), which allows users to examine structural data via stereographic projections. These analyses were performed using the lower hemisphere stereographical projection method as illustrated by Hoek and Bray (1981) and Goodman (1989). This programme was used to investigate potential rock slope failure modes including planar sliding, wedge sliding, flexural toppling and direct toppling. Apart from selection of failure mode, the slope orientation, friction angle and lateral limits were also specified. The slope orientations for profiles *A*, *B* and *C* were 133°, 81° and 230°, respectively (Table 4), whereas the friction angle and lateral limits for all profiles were 35° and 20°, respectively (Consultant D, 2011). The orientation columns in the data file were interpreted as dip and dip direction values and the declination remained at zero as it was assumed that all measurements were recorded by considering this adjustment (Consultant D, 2011). Windows were drawn around data clusters of pole vectors and contour plots to obtain mean orientations (Table 4). These were then plotted as both poles and planes and were subsequently employed in the kinematic analysis. This analysis was carried out for both the overall slope angle of 57° and the stack angle of 76°, as described by Consultant D (2011). The kinematic analysis overlays the respective failure modes, and was subsequently displayed on the stereonet in order to investigate whether or not failure is kinematically feasible.

The combined data employed in the kinematic analysis were obtained by Consultant C (2009) and Consultant D (2011). The data comprised details on the feature type, dip and dip direction, persistence, roughness, aperture and infilling. Discontinuity orientation measurements were also collected from Sirovision 3D photographs for areas which were not easily or safely accessible. Hand measurements took place at 5 different faces located throughout the entire pit, whereas Sirovision measurements were taken at three of these faces and an additional two elsewhere in the pit.

The type of features measured by Consultant D (2011) consisted of shear zones, mylonite zones, normal faults, dykes, contacts, veins including pegmatite veins, and joints. The total number of each type was 87, 8, 50, 28, 3, 65 and 562, respectively. The major discontinuities were selected based on their levels of influence, which were considered to be joints with a persistence exceeding 3 m as well as major structures including shears, dykes, veins and faults. With such filters, there are 86 shear zones, 8 mylonite zones, 50 normal faults, 28 dykes, 3 contacts, 63 veins, 191 joints and 54 Sirovision measurements. The 5 main discontinuity sets identified by Consultant D (2011) were based on measurements across the entire pit shell and were further employed in a rockfall hazard analysis. The major discontinuity sets in this study, however, were based on discontinuity measurements of 3 of 9 mapping areas in which the 3 critical profiles were selected. This was attributable to the potential overshadowing effect by the larger quantity and variability of discontinuity measurements. Set windows were drawn based on pole and contour plots and their mean orientations were plotted as both poles and planes (Table 4).

3.5. Numerical modelling

Two types of geotechnical models were explored, i.e. continuum and pseudo-discontinuum approaches. For the pseudo-discontinuum approach, main joint sets responsible for potential planar and wedge failures, determined using the LEM, were incorporated into profiles as 2D joint networks in order to test the identified structurally controlled failure modes. By simplifying the structural data, joints were incorporated into finite element models as parallel deterministic and Veneziano joint network models (Veneziano, 1978). The former was applied as joints of infinite length and the latter as joints of finite length with rock bridges introduced along discontinuity planes. Results were compared to those produced in FLAC (Itasca, 2011) using the ubiquitous joint network model due to similarities in joint spacing, length and density. In order to introduce stochastic and thus more realistic joint conditions, the Veneziano joint network (Veneziano, 1978)

was employed. This model was selected to represent potentially unstable joints since Dershowitz and Einstein (1988) found that the Poisson line process, on which it is based, corresponded well with observed rock joint systems in a number of rock masses.

The rock mass in the continuum approach was modelled as a linear elastic-perfectly plastic material through application of both the generalised Hoek–Brown strength criterion (Hoek et al., 2002) and equivalent Mohr–Coulomb parameters determined from a range of minor principal stress values defined by $\sigma_t < \sigma_3 < \sigma'_{3max}$. σ'_{3max} is the maximum value for the minor principal stress (Hoek et al., 2002). In contrast, materials were modelled solely with equivalent Mohr–Coulomb parameters for pseudo-discontinuum approaches since the ubiquitous joint network model restricts the use of this constitutive model. The orientation of ubiquitous joints also corresponded to the potentially unstable conditions determined by the major joint sets responsible for plane and wedge failures using the LEM (Romer, 2017). The strength properties of the rock mass associated with these criteria were estimated in software package RocLab (Rocscience Inc., 2015) by utilising the combined data from Consultant A (1996), Consultant B (2006), Consultant C (2009) and Consultant D (2011).

3.5.1. Discrete fracture network in pseudo-continuum media

The 2D finite element analysis code RS2 (Rocscience Inc., 2015) is an implicit continuum model that was employed with the shear strength reduction (SSR) technique to analyse the stability of the three critical profiles. The modelling or pre-processing module of Phase2 (Rocscience Inc., 2015) allowed for the building of models by introducing and adapting the geometry of the problem domain, specifying stresses, defining material and discontinuity properties, generating finite element mesh, and finally specifying boundary conditions. All analyses were performed under plane strain conditions where the major and minor principal stresses (σ_1 and σ_3, respectively), out-of-plane principal stress (σ_z), and in-plane displacements and strains were calculated. The Gaussian elimination solver type was employed in all analyses. For stress analyses, a maximum number of 500 iterations were specified and an automatic number of load steps were selected. The absolute energy convergence type was adopted. The initial estimate of the SRF was set to 1 and an automatic step size was employed. The initial in situ stress imposed on all models was the gravitational field stress which made use of the actual model ground surface to calculate the depth below it. A total stress ratio k (defined as the ratio of horizontal to vertical stress in the in-plane and out-of-plane directions) of 1 was used for all analyses. The horizontal stress at the surface, also referred to as the locked-in horizontal stresses (in-plane and out-of-plane directions) remained as zero in all models. A uniform finite element mesh was employed in all models which defines approximately equal-size elements throughout them. Six-noded triangle elements were used as they incorporate mid-side nodes to enhance results (13,700 elements). The displacement boundary conditions were specified next. Pinned boundary conditions suggest that the boundaries are unable to move in the x- and y-direction and thus maintain a zero displacement during analysis. Such conditions were applied to all external boundaries except for those representing the ground surface, which was instead characterised as free boundaries. The type of initial element loading was specified as 'field stress and body force' where field stress refers to the stress properties previously specified in the loading properties, and body force represents the self-weight of elements derived from the material unit weight to be specified. The strength properties employed include the failure criterion, material type, tensile strength, friction angle and cohesion of each material presented in the profile. The generalised Hoek–Brown strength criterion and associated parameters were employed in the analysis of profiles without discontinuities. Equivalent Mohr–Coulomb strength parameters, however, were employed in both discontinuum and continuum models. The elastic properties used, Young's modulus (E_m) and Poisson's ratio (ν), are those associated with good quality rock masses, as listed in Tables 1 and 2.

3.5.2. Finite difference method in pseudo-discontinuum media

FLAC (Itasca, 2011) was operated in menu-driven mode via the GIIC (graphical interface for Itasca codes). The external and material boundaries defining the problem geometry were imported as DXF files using the 'Sketch' tool. The 'Cleanup' stage of this tool was then employed to eliminate or merge any non-essential vertices from the sketch. Next, the boundaries were copied to the geometry builder in order to construct quadrilateral zones. In the geometry builder, the 'Create' stage was used to produce additional construction lines in order to partition the problem domain into several four-sided blocks which are subsequently filled with zones. The 'Cleanup' stage was used to remove erroneous lines or vertices. In the 'Blocks' stage, block points were marked manually to create the four-sided blocks which then enclosed the mesh. The 'Edit' tool was employed for modifying the virtual grid. Here, the 'Boundary' stage was used to assign external automatic boundary conditions where roller and pinned conditions were applied to the sides and bottom of the virtual grid, respectively. The 'Mesh' stage was subsequently used to adjust the zone density to a predefined average total number of 60 horizontal zones which by default represents a fine mesh. Once the virtual grid was created, the 'Execute' action sent the newly defined commands to FLAC (Itasca, 2011). In the case of a slightly poor aspect ratio of individual zones, additional improvements were made via the 'Shape' stage of the 'Alter' tool. Here, points were manually selected and shifted to enhance the zone ratios. Material properties were then assigned to various geological materials based on the predetermined constitutive models (Tables 1 and 2). In this study, the Mohr–Coulomb and Hoek–Brown constitutive models were selected in a plastic state. Once a material was selected via a rectangular range, the properties were inserted. Thereafter, the gravitational acceleration was incorporated into the model via the 'Gravity' tool. Gravity was defined in terms of magnitude and direction angle and was specified automatically. Following the generation of the model, the 'Solve' stage of the 'Run' tool was employed to calculate a steady-state equilibrium solution which was followed by a safety factor calculation via the 'SolveFoS' stage. FLAC variables were then superimposed to create a model plot of the calculation results. Using the 'Model' stage of the 'Plot' tool, the model boundary, safety factor, maximum shear strain and plasticity indicators were selected from the item tree and the plots were created and exported.

4. Results

4.1. Ubiquitous joint network

In order to account for the presence of weak planes in the finite distinct element model, i.e. Mohr–Coulomb model, joint networks were simulated via the ubiquitous joint network model. Two joint set inclinations were analysed separately, and the inclination selection was based on critical main joint sets that predicted planar and wedge failures.

In profile *A*, joints sets incorporated into the model include J1 and J3 having inclinations of 81° and 57°, respectively. The maximum shear strain contours associated with these inclinations are shown in Fig. 9a and c. At joint inclination of 81°, the obtained safety factor was 2.52 (Table 5). The maximum shear strain of 2.5×10^{-4} occurred along the dolerite-metagabbro boundary and

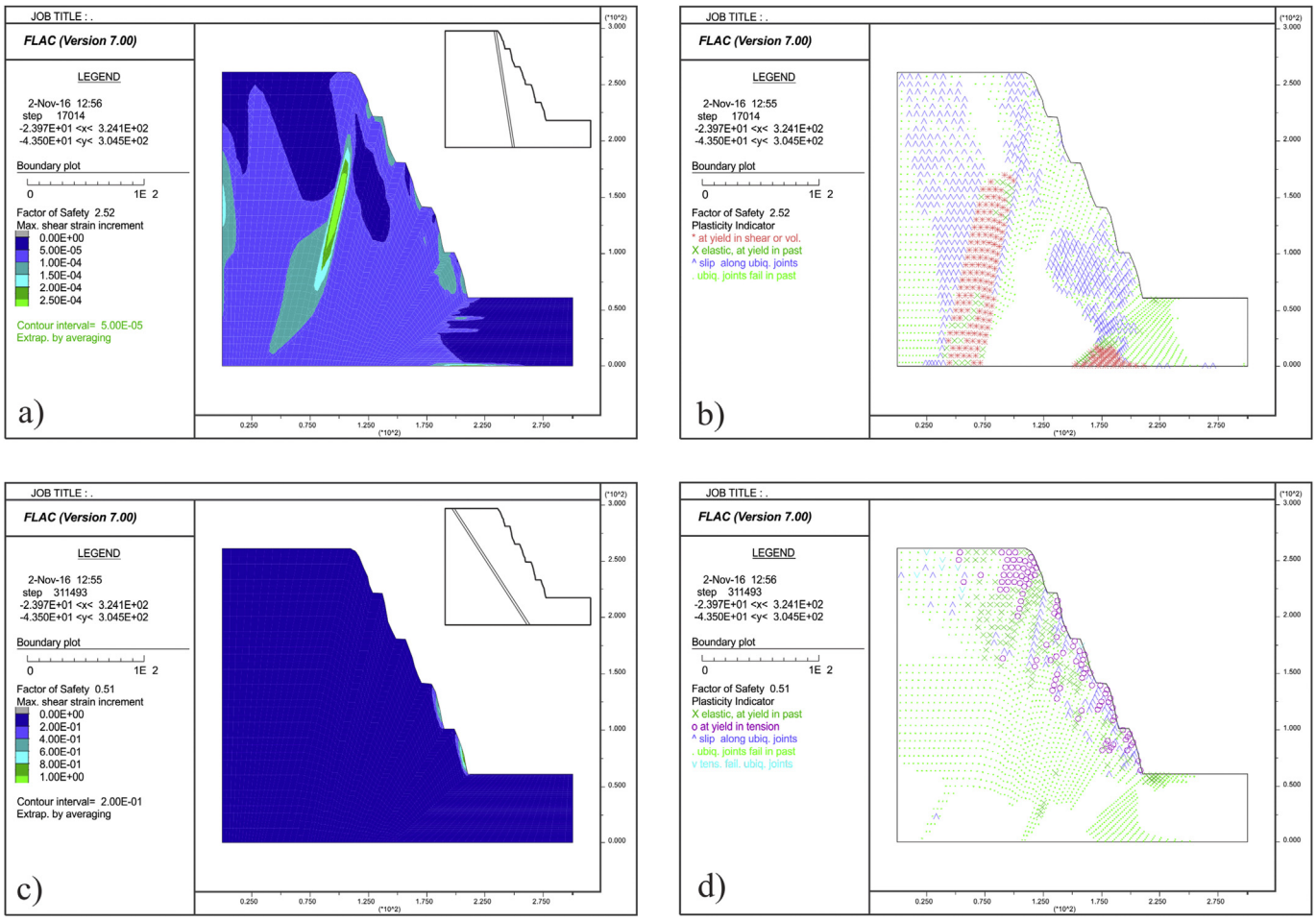

Fig. 9. Results of the FDM with the ubiquitous joint network model for (a) profile *A* with an inclination of 81° (J1) and (b) its associated plasticity indicators, and (c) profile *A* with an inclination of 57° (J3) and (d) its associated plasticity indicators.

gradually diminished to the outer boundaries of the model (Fig. 9a). The plasticity indicators show that this area is dominated by slip along ubiquitous joints (Fig. 9b). When employing a joint inclination of 57°, very different results are obtained. The calculated safety factor was 0.51 (Table 4) and the highest shear strain of 1 occurred along thin bands at the slope faces of the two bottom benches (Fig. 9c). Upon examination of the yielded elements, it is evident that tensile failure occurs at these locations (Fig. 9d). Tensile failure along ubiquitous joints is apparent at bench crests whereas slip along ubiquitous joints occurs predominantly throughout each bench (Fig. 9d).

In profile *B*, joint sets J1 and J2 were applied to the ubiquitous joint model and had an inclination of 56° and 44°, respectively. Safety factors of 0.65 and 1.01 were computed for joint sets J1 and J2, respectively (Table 4). Results using an inclination angle of 56° reveal an indication of planar failure along the slope face of the uppermost bench where the highest shear strain of 4 occurs (Fig. 10a). Yielded elements in this location show a combination of slippage along ubiquitous joints as well as tension (Fig. 10b). With a joint inclination of 44°, the highest shear strain of 8×10^{-4} arises along the uppermost and lowermost benches. There is evidence of the formation and propagation of tensile cracks behind the crest as well as a deep-seated approximately planar failure surface created from the corner of the external boundary farthest away from the slope face and extending down to the toe of the slope (Fig. 10c). Yielded elements also indicate slip along uqibuitous joints (Fig. 10d).

In profile *C*, joint sets J1 and J2 with inclinations of 53° and 87°, respectively, were incorporated into FDM models. Safety factors of 0.8 and 1.57 were computed for joint sets J1 and J2, respectively (Table 4). At joint inclination of 53°, the sliding plane daylights out of the overall slope and bench face, suggesting the formation of rigid blocks sliding along these planar joints. The maximum shear strain of 0.01 occurs at the uppermost bench face and extends slightly into the slope. A similar pattern is observed on all successive benches. Shear strain contours also suggest the presence of a tensile crack starting behind the slope crest (Fig. 11a). According to the plasticity indicators in Fig. 11b, the bench floors are associated with tension whereas the bench face slopes coincide with slip along ubiquitous joints. Non-daylighting joints such as J2 result in a failure mode involving sliding along ubiquitous joints and shearing through the rock mass (Fig. 11d). The maximum shear strain of 3.5×10^{-4} is observed at the vertical external boundary away from the slope face. No single clear failure plane is presented but several thin bands are shown across the profile instead (Fig. 11c). The bands bordering the slope face represent shear zones as opposed to the deep-seated bands which represent zones where sliding occur along the ubiquitous joints. Shearing is confined within the tonalite material boundaries whereas sliding occurs within metagabbro (Fig. 11d).

Table 5
Safety factors obtained for pseudo-discontinuum media using the FEM and FDM.

Profile	Joint set	Parallel deterministic joint network		Ubiquitous joint network	Veneziano joint network
		Infinite length	Finite length		
A	J1	2.89	4.51	2.52	4.73
	J3	0.52	4.45	0.51	4.6
	J1 and J3	0.75	3.77	–	4.34
B	J1	0.41	5	0.65	4.3
	J2	0.7	5.27	1.01	4.98
	J1 and J2	0.46	4.42	–	4.64
C	J1	0.65	4.27	0.8	4.48
	J2	3.44	4.55	1.57	4.51
	J1 and J2	0.76	3.84	–	4.22

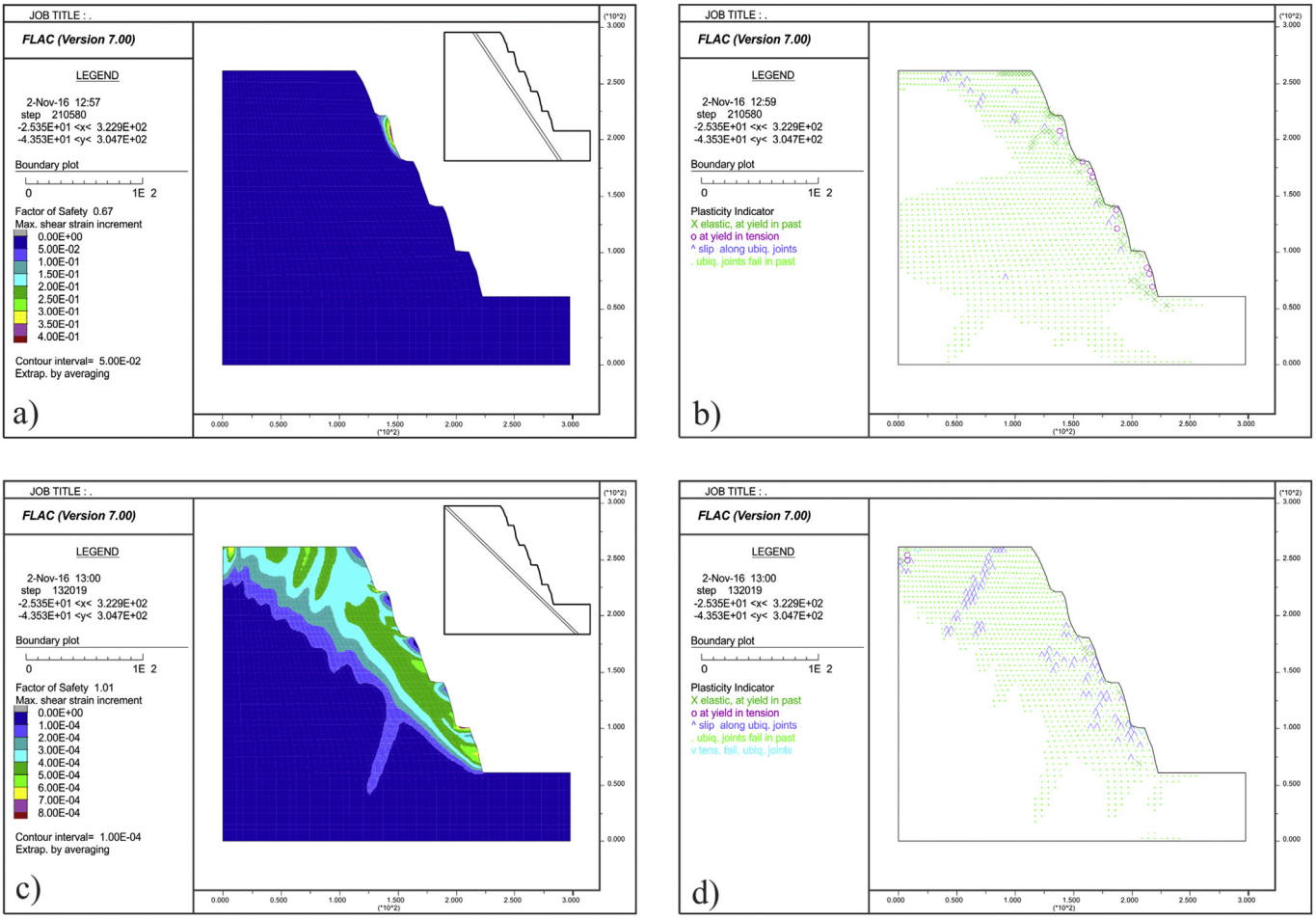

Fig. 10. Results of the FDM with the ubiquitous joint network model for (a) profile *B* with an inclination of 56° (J1) and (b) its associated plasticity indicators, and (c) profile *B* with an inclination of 44° (J2) and (d) its associated plasticity indicators.

4.2. Parallel deterministic joint network

The parallel deterministic joint network also applied critical joint sets responsible for potential plane and wedge failures individually and simultaneously. This was conducted assuming discontinuities to be of infinite length and subsequently of finite length, having a persistence of 0.8. This value is indicative of the uniform length of rock bridges occurring between each joint segment where a value close to 1 implies near infinite length and a value closer to 0 suggests a near continuum material. This value was selected for comparative purposes with the ubiquitous joint network model in the finite distinct element model.

Joint set J1 (81° dip) in profile *A* shows a similar failure surface to that observed in FDM where the maximum shear strain of 2.4×10^{-3} occurs along the dolerite-metagabbro interface and is dominated by shear failure (Fig. 12a). The safety factor was found to be 2.89 (Table 5). Most horizontal displacements associated with this joint angle occur in the vicinity of the second and third lowermost benches and extend to the metagabbro-dolerite contact where the band of maximum shear strain exists. For joint set J3, however, the maximum shear strain of 1.7×10^{-4} occurs at the toe of the slope followed by the centre of the profile where the yielded elements are confined to the upper portion of the dolerite dyke (Fig. 12b). A safety factor of 0.52 was calculated and the highest

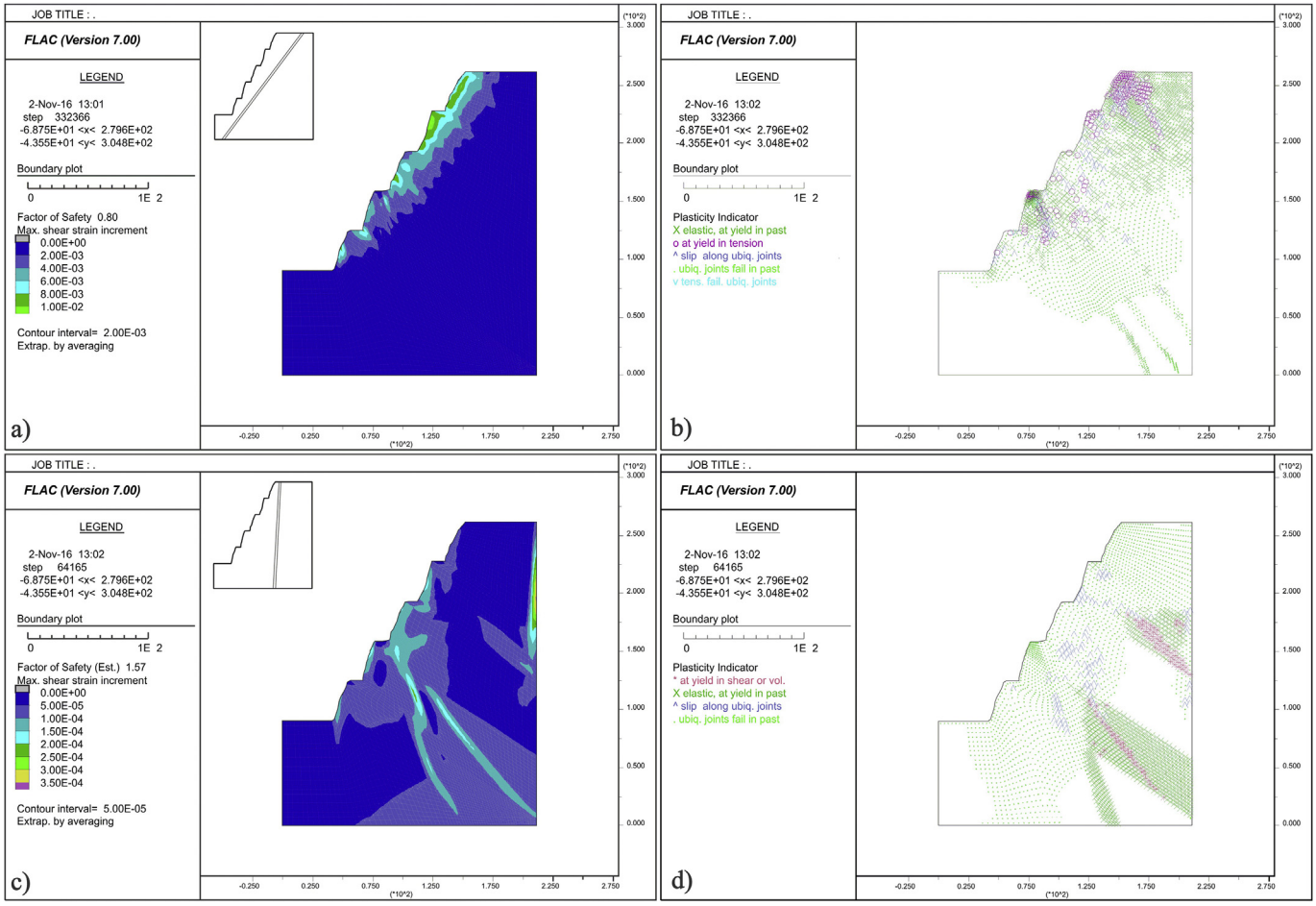

Fig. 11. Results of the FDM with the ubiquitous joint network model for (a) profile *C* with an inclination of 53° (J1) and (b) its associated plasticity indicators, and (c) profile *C* with an inclination of 87° (J2) and (d) its associated plasticity indicators.

degree of horizontal displacement is limited in the uppermost bench. When both joint sets are combined into a single model, similar results to those of J3 are obtained in terms of shear strength (Fig. 12b and c), and a safety factor of 0.75 is achieved. The largest displacements, however, arise at the slope crests as well as along the two succeeding bench faces and follow J3 (58°). In profile *B*, similar shear strain contours are obtained for both joint sets J1 and J2, as well as a combination of J1 and J2 where the maximum strain exists at the toe of the slope (Fig. 12d–f). The maximum horizontal displacements are also near identical between the three models, occurring on the floor and slope face of the uppermost bench. The safety factors determined for J1, J2 and J1 and J2 combination were 0.41, 0.7 and 0.46, respectively (Table 5). Tensile failure is the main failure mode and is more prevalent at a joint angle of 44° in comparison to the other two angles. When applying a joint set angle of 53° (J1) in profile *C*, no clear failure surface arises from shear strength contours (Fig. 12g), but since the joint set daylights in the slope face, the failure mode is expected to be in tension. On the contrary, J2 (87°) has a non-daylighting inclination where sliding on discontinuities and shearing through the rock mass occur. Several irregular bands can be observed from the shear strain contour plot (Fig. 12h). When combining both sets, the shear strain contours do not reveal a definite sliding plane, but the largest strain is experienced at the toe of the slope (Fig. 12i). Yielded elements occur along bench floors and slope faces and signify failure in tension. The safety factors determined for J1, J2 and J1 and J2 combination were 0.65, 3.44 and 0.76, respectively (Table 5).

Rock bridges were introduced into the models through application of joints of finite length having a persistence of 0.8. In profile *A*, safety factors for J1, J3 and J1 and J3 combination were 4.51, 4.45 and 3.77, respectively (Table 5). The shear strain contours for all three situations show faint signs of the onset of circular failure, but the maximum strain continues to be confined to the upper boundary of the dolerite dyke when joint sets are analysed individually (Fig. 13a–c). In profile *B*, the safety factors for J1, J2 and J1 and J2 combination were 5, 5.27 and 4.42, respectively (Table 5). The shear strain contours show well defined circular failure planes when joint sets are analysed independently (Fig. 13d–f). In profile *C*, the safety factors computed for J1, J2 and J1 and J2 combination were 4.27, 4.55 and 3.84, respectively (Table 5). Shear strain contours are again more noticeable when joint sets are analysed independently (Fig. 13g–i). Although multiple failure surfaces are shown for individual J1 and J2, there is a vague sign of circular failure for all three situations (Fig. 13g–i).

4.3. Veneziano joint network

The Veneziano joint network model was incorporated to introduce more realistic joint conditions due to the introduction of joints which vary in terms of orientation and inclination, and the joint lengths are based on an exponential statistical distribution.

In profile *A*, the safety factors produced through applications of J1, J3 and J1 and J3 combination were 4.73, 4.6 and 4.34, respectively (Table 5). The maximum shear strain follows the upper

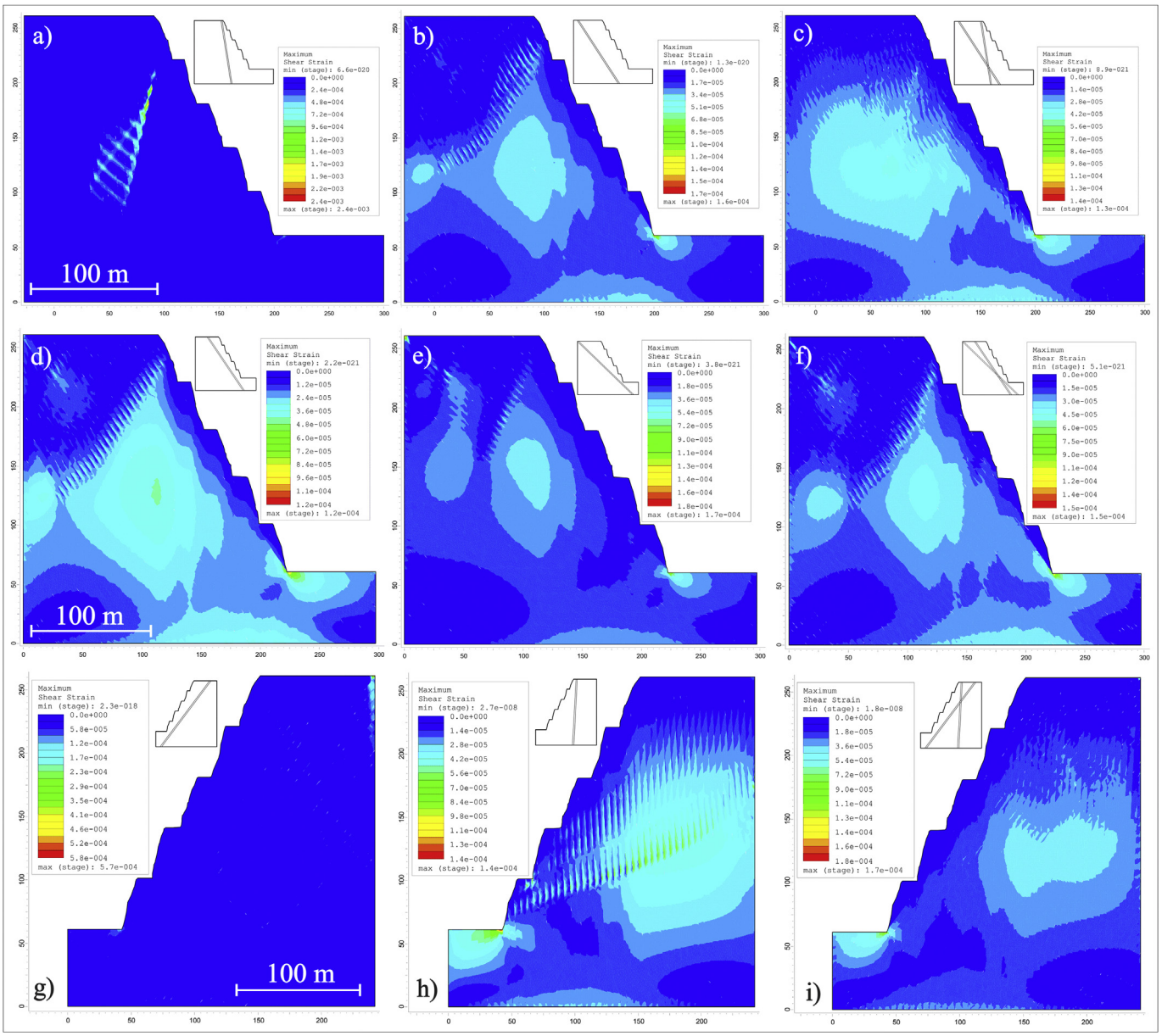

Fig. 12. Maximum shear strain associated with the parallel deterministic joint network of infinite length showing (a) profile *A* with J1, (b) profile *A* with J3, (c) profile *A* with combined J1 and J3, (d) profile *B* with J1, (e) profile *B* with J2, (f) profile *B* with combined J1 and J2, (g) profile *C* with J1, (h) profile *C* with J2, and (i) profile *C* with combined J1 and J2.

boundary of the dolerite dyke when assessing J1 and a combination of J1 and J3 (Fig. 14a and c). In all three cases, however, there is an indication of an approximately circular plane extending from the overall slope crest to toe (Fig. 14a–c). In profile *B*, the safety factors produced through applications of joint J1, J2 and J1 and J2 combination were 4.3, 4.98 and 4.64, respectively (Table 5). All three cases show that the maximum shear strain occurs along a thin circular band extending through the slope (Fig. 14d–f). In profile *C*, the safety factors produced through applications of J1, J2 and J1 and J2 combination were 4.48, 4.51 and 4.22, respectively (Table 5). The maximum shear strain occurs along multiple approximately circular planes when assessing J1 and J2 independently (Fig. 14g–i).

5. Discussion

In this study, we investigated the effect of natural discontinuities on rock slope stability conditions using common commercial code where geotechnical engineering practitioners can easily access. We adopted the whole process, from analysis of filed collected data (window mapping and Sirovision measurements), to kinematic analysis and definition of the most critical joint sets, and further to the numerical simulation using 2D stochastic fracture traces embedded in FDM or FEM models. Three critical profiles were analysed using a variety of joint networks which form the pseudo-discontinuum media or effective continiuum media. The joint networks range from having joints of infinite lengths across the profile to those of finite lengths where rock bridges are introduced along joint planes by altering joint persistence to 0.8.

5.1. Safety factor

The results of the analysis based on the three profiles representing pseudo-discontinuum media can be compared among various joint network models employed. In all profiles, there is a

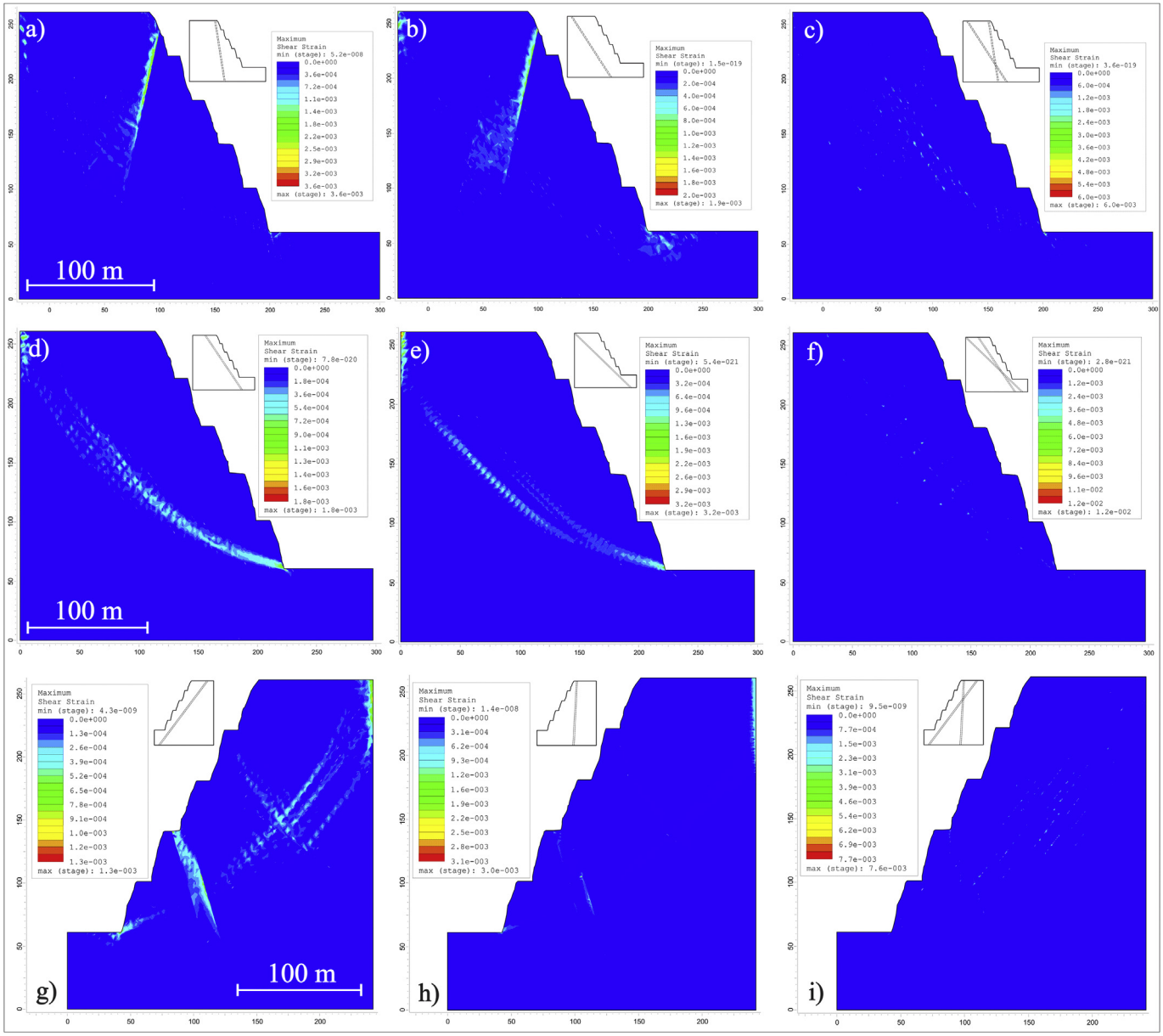

Fig. 13. Maximum shear strain associated with the parallel deterministic joint network of finite length showing (a) profile *A* with J1, (b) profile *A* with J3, (c) profile *A* with combined J1 and J3, (d) profile *B* with J1, (e) profile *B* with J2, (f) profile *B* with combined J1 and J2, (g) profile *C* with J1, (h) profile *C* with J2, and (i) profile *C* with combined J1 and J2.

good correlation in safety factors obtained between the parallel deterministic infinite and ubiquitous joint models, as well as between the parallel deterministic finite and Veneziano joint models (Fig. 15). It is also found that the former correlates well with the structurally controlled limit equilibrium model and the latter with the stress controlled limit equilibrium model. The structurally controlled limit equilibrium model, however, seems to underestimate safety factors, whereas the stress controlled limit equilibrium model generally overestimates the safety factors (Romer, 2017; Romer and Ferentinou, 2017). It should be noticed that the analysis, based on persistence of 0.8 in the parallel deterministic finite and the Veneziano joint models, resulted in higher resistance to shearing and therefore stress-controlled failure mechanism.

For profile *A*, comparable safety factors are calculated via the parallel deterministic infinite and the ubiquitous joint models for J1 and J3 (Fig. 15). In both joint network models, J1 suggests stable conditions as opposed to J3 that yields unstable conditions. These results agree with those of the structurally controlled limit equilibrium model where planar failure along J3 was probable at both overall and stack angle levels having safety factors of 0.93 and 0.72, respectively (Romer, 2017; Romer and Ferentinou, 2017). When incorporating a combination of joints J1 and J3 via the finite element pseudo-continuum model, unstable conditions are presented with a safety factor of 0.75 (Fig. 15).

For profile *B*, safety factors produced via the parallel deterministic infinite and the ubiquitous joint models indicate unstable conditions for all three joint orientation conditions (safety factor of 0.41–0.7), apart from J2 for the ubiquitous model which suggests a critically stable slope (safety factor of 1.01). Very similar values are computed for individual sets J1 and J2 where the minimum safety factors are computed by the parallel deterministic infinite model. When combined sets J1 and J2 are incorporated into the model such as the parallel deterministic infinite model, stable slopes (safety factor of 4.3–5.27) are computed for all joint orientation conditions

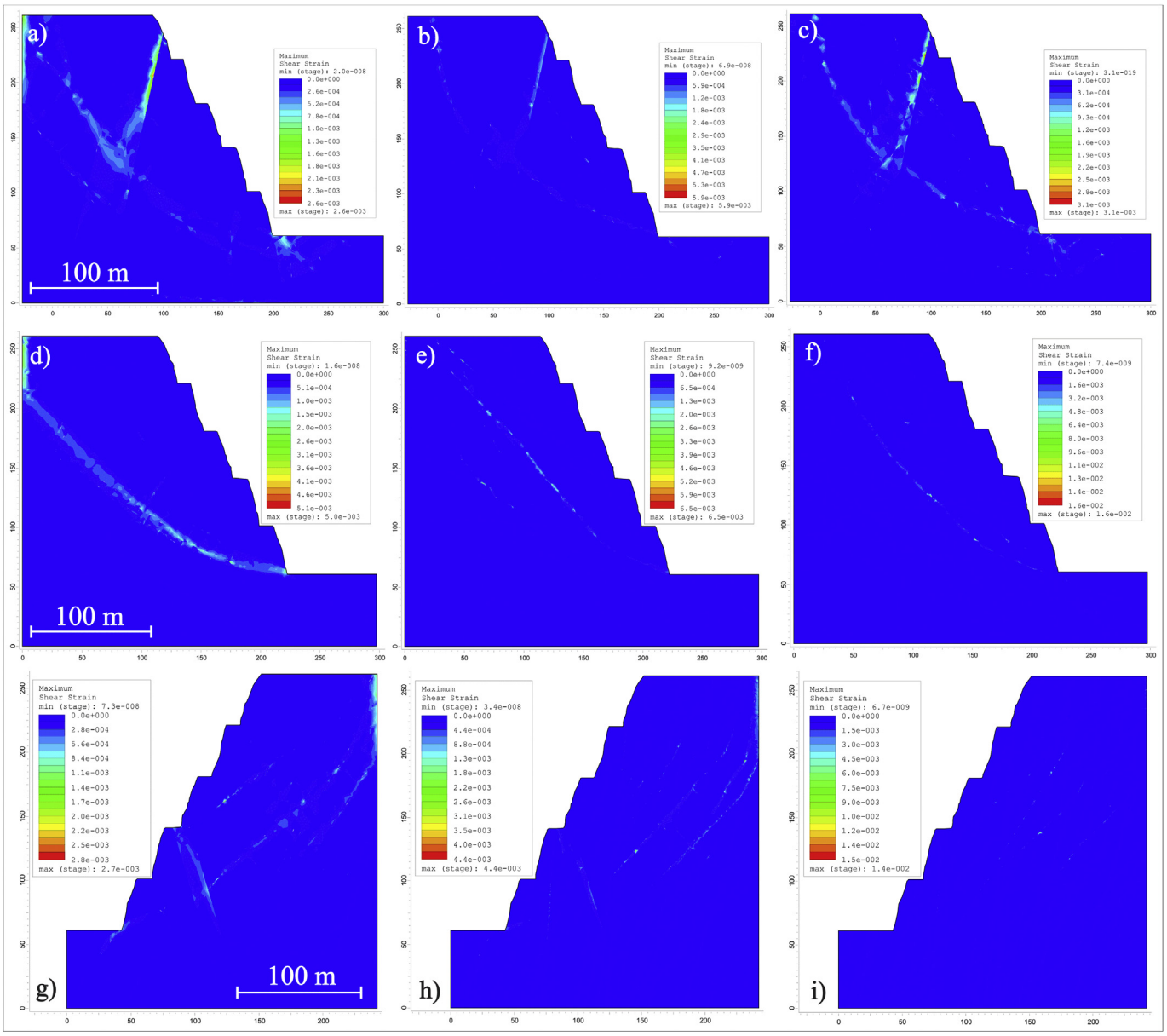

Fig. 14. Maximum shear strain associated with the Veneziano joint network for (a) profile *A* with J1, (b) profile *A* with J3, (c) profile *A* with combined J1 and J3, (d) profile *B* with J1, (e) profile *B* with J2, (f) profile *B* with combined J1 and J2, (g) profile *C* with J1, (h) profile *C* with J2, and (i) profile *C* with combined J1 and J2.

applied to the parallel deterministic finite and the Veneziano models, the lowest value of which is associated with J1. Very similar values are computed between the two joint networks for J2 and J1 and J2 combination.

For profile *C*, the parallel deterministic infinite model and the ubiquitous joint network produce similar safety factors for J1 but a difference of 37% arises for J2 (Fig. 15). Individual sets J1 and J2 indicate stable and unstable conditions, respectively, in both cases. Stable conditions are calculated for joint orientation conditions applied as the parallel deterministic finite and the Veneziano models (Fig. 15). There is a good agreement in values obtained by these two joint networks for all three joint orientation conditions.

5.2. Failure surfaces and strain distribution

For profile *A*, similar strain accumulation zones are achieved using the FEM with the parallel deterministic infinite model and the finite distinct element method with the ubiquitous joint network at an angle of 81° (J1) where the maximum shear strain occurs midway down the dolerite dyke. This failure mode is, however, not evident using the parallel deterministic finite model where the maximum shear strain occurs at the centre and toe of the slope. By applying the combined sets J1 and J3 in this model, shear strain contours do not define a single sliding plane; however, there is an obvious sign of slip along J3. For the parallel deterministic infinite and the Veneziano models, the maximum shear strain accumulation continues to be confined by the contacts of the dolerite dyke, yet the manifestation of a circular failure surface is also evident for all three joint orientation conditions, particularly for the Veneziano model.

For profile *B*, the resulting failure mode associated with J1 using the ubiquitous joint is the planar failure along the uppermost bench. When applying J2 to the model, however, shear strain contours form a large planar failure surface from tensile cracks developed behind the crest to the toe of the slope where the maximum strain is accumulated. With applications of J1, J2 and J1

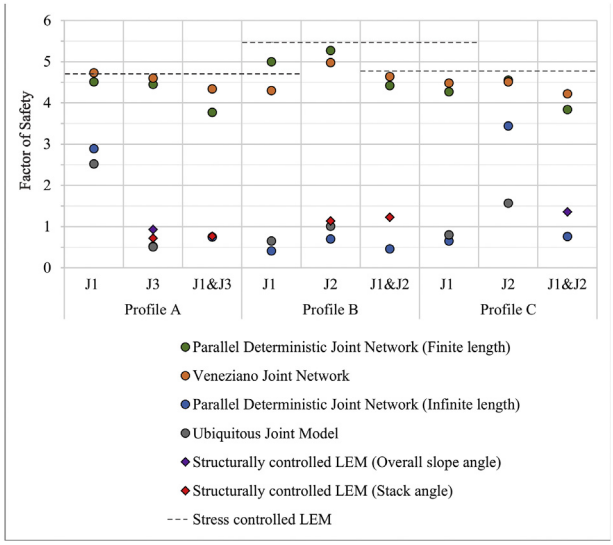

Fig. 15. Safety factors produced for pseudo-discontinuum media using various joint networks.

and J2 combination in the FEM with the parallel deterministic infinite model, there is no definitive failure mechanism. Shear strain accumulates in the centre of the profile and at the toe of the slope with slip occurring along the respective joints and along J1 for J1 and J2 combination. The resulting shear strain accumulation associated with the parallel deterministic infinite and Veneziano models of J1 indicates deep-seated curved failure surfaces and develops into less defined and more planar surfaces with applications of J2 and a combination of J1 and J2.

For profile *C*, application of J1 as the ubiquitous model of the FDM depicts strain accumulation along bench faces and strain contours extending into the slope to form potential toppling blocks. A different result is obtained using the parallel deterministic infinite model where strain accumulates in the centre and at the toe of the slope. Shear strain contours for J2 is, however, comparable between the two joint networks where the maximum strain accumulates within the dolerite intrusion. Similar failure surfaces are predicted using the parallel deterministic finite and the Veneziano models but with the addition of curved failure surfaces. These are less distinct using the latter joint network model and also become less apparent when both joint sets are combined into a model.

It is clear that the parallel deterministic infinite and ubiquitous joint models have a significant effect on the stability of slope. In a comparative study between parallel deterministic, parallel statistical, cross jointed, Baecher, Veneziano and Voronoi joint networks all having an identical orientation, spacing and density, it was found that the parallel deterministic joint network produced the largest SRF since the shear strength of rock masses was increased due to the lack of connection in the parallel joints (Moradi and Hosseinitoudeshki, 2015). According to Terzaghi (1962), a reduced spacing between continuous joints leads to these joints having an increasing influence on the stability of slopes. The intensely jointed profiles (spacing of 5 m) in relation to the scale of the slope could thus be the cause of the reduced safety factors. In reality, however, most rock masses contain discontinuous joints varying in persistence, length and spacing. The use of joint networks with the introduction of rock bridges suggests stable conditions. According to Terzaghi (1962), most cohesion in such jointed rock masses occurs in these gaps between disrupted joint planes. A shear failure along a plane comprising both joints and intact material is resisted by the combined effects of pressure-conditioned shear resistance and the cohesion of the intact material. The developed near circular failure surfaces exhibited by most profiles using the parallel deterministic finite and Veneziano models could be due to the intensity of jointing where Bye and Bell (2001) stated that circular failures are possible in highly fractured rock masses which could be considered to be randomly jointed and isotropic. Despite the fact that the presence of rock bridges could aid in stabilising a rock slope, failure remains a possibility due to a potential buildup of shear stresses resulting from an increasing slope height which may cause the gradual elimination of these rock bridges through their breakup thus causing a decrease in cohesion (Terzaghi, 1962). Tensile failure of intact rock bridges is typically the primary failure mode (Einstein et al., 1983; Einstein, 1993; Shen, 1993) followed by shear fracturing as the secondary mode (Sjöberg, 1999). With the advent of more joints becoming free to open progressively, the distribution of normal stresses on joint walls gradually becomes irregular causing local stress accumulation on blocks located between these joints and eventually their failure (Terzaghi, 1962).

It has been recognised that a nonlinear relationship exists between shear and normal stresses of rock masses, particularly at lower stress levels corresponding to that of surface conditions. The estimate of equivalent Mohr–Coulomb strength parameters conforming to a nonlinear criterion is thus essential in practice. The method proposed by Hoek et al. (2002), in which a range of minor principal stress values corresponding to a specified slope height and unit weight was employed in calculation of equivalent Mohr–Coulomb parameters, was evaluated in this study. It was proven to be effective in terms of calculating comparable safety factors in both non-structurally controlled limit equilibriums and numerical models with only marginal variations. Furthermore, analogous shear strain accumulation zones and shear strain values were found between the strength criteria using the FEM and FDM. Discrepancies in failure surfaces arose between the limit equilibrium and numerical models for profiles consisting of multiple materials.

With the validation of appropriate Mohr–Coulomb strength parameters, they were extended to the analysis of pseudo-discontinuum or equivalent continuum media where joints were integrated into previous continuum and intact media. The reason behind this was the limitation of the FDM code FLAC which is restricted to the use of the Mohr–Coulomb criterion in conjunction with the ubiquitous joint network model. Closely spaced joints with continuous or near-continuous joint lengths such as those of the parallel deterministic joint network of infinite length and the ubiquitous joint network model revealed that the stability of slopes was structurally controlled where safety factors were found below 1.5 mostly, comparable to those of the predicted failure modes in the structurally controlled slopes in the LEM. It was also found that planar failure and/or wedge sliding were common at stack angle level whereas planar and toppling modes were typically associated with the entire pit slope. Contrasting results come about in terms of shear strain accumulation zones between the continuum methods, where the FDM depicts recognisable failure modes correlated to that of the LEMs while the FEM portrays widely distributed strains with slippage along joints.

In reality, rock masses typically comprise joints of a discontinuous nature which vary with regard to orientation, length, persistence and spacing. With a change in discontinuity persistence and a corresponding increase in the amount of intact material in the form of rock bridges along discontinuity planes, the parallel deterministic joint network of finite length revealed that stability was significantly enhanced. Stochastic and more realistic joint conditions in which all aforementioned joint properties were statistically randomised were assessed via the Veneziano joint network model. Similar results to those of the parallel deterministic infinite model were produced in terms of both safety factors and shear strain

accumulation zones. Due to the high degree of fracturing in relation to the profile scale, the failure surfaces described by the shear strain accumulation zones indicated approximately circular surfaces which followed lines of least resistance.

The applied models neglect 3D effect, or step-path 'en echelon' failures, and progressive sliding surface development, related to crack initiation, propagation, coalescence and degradation to failure. Yet it is clear from the analysis that a small variation of persistence even in simple pseudo-discontinuum models produces large variations in slope resistance and expected failure. This study confirms that uncertainty of persistence could yield completely different results and drive the designer to be conservative and assume 100% persistence. The common assumption of 100% persistence, based on field evidence, could be conservative in terms of strength and stiffness, but may be misleading.

As discussed in Hoek (1999) and Read and Stacey (2009), the foundation of any practical rock engineering analysis is a good geological model and the geological data upon which the definition of structural discontinuities is based. Elmo et al. (2018) reminded that despite the very narrow range of geological conditions that may yield truly 2D rock bridges, most rock bridge problems in the published literature are 2D simplifications. It is therefore necessary that the engineers consider carefully the inherent limitations that a simplification from 3D to a 2D fracture analysis is entailed. The same authors suggested that a rock bridge analysis based on a given section plane and multiple (stochastic) 2D joint networks can be used to address the issue related to the location of the section plane (e.g. Einstein et al., 1983; Elmo et al., 2011; Dershowitz et al., 2017). Stochastic based step-path models generally assume a constant stress field condition to estimate the normal stress component acting on each existing fracture in the model. Under this limit equilibrium assumption, the potential failure paths would represent a scenario in which the rock bridges would have the same probability of failure and, under those circumstances, failure would involve all rock bridges simultaneously. However, as this is not well supported by the literature, Elmo et al. (2018) proposed that a stochastic approach would work better when integrated with a numerical analysis capable of considering progressive rock mass damage and changes in stresses within the rock slope. The hybrid methods, which combine continuous and discontinuous methods (e.g. numerical manifold method to model progressive failure) are likely to provide a more comprehensive analysis (Wong and Wu, 2014).

6. Conclusions

The major conclusions drawn from this context are presented as follows:

(1) The introduction of rock bridges along closely spaced and parallel discontinuity planes significantly enhances stability. A similar relationship is found with additional joint property variations (i.e. orientation, spacing, and length). Due to the high degree of fracturing in relation to the profile scale, the failure surfaces described by the shear strain accumulation zones indicated approximately circular surfaces, which followed lines of least resistance.
(2) Planar failure and/or wedge sliding are common at stack angle level, whereas planar and toppling modes are typically associated with overall pit slope angles. Potential toppling failure modes at overall pit slope angles are revealed in numerical analyses, along joint orientations which were not considered in the LEMs.
(3) Closely spaced joints with continuous or near-continuous joint lengths in equivalent continuum numerical models revealed that the stability of slopes is structurally controlled, where most safety factors were found to be less than 1.5.
(4) The estimation of equivalent Mohr–Coulomb strength parameters conforming to the nonlinear generalised Hoek–Brown failure criterion, based on a range of minor principal stress values, was proven to be effective in terms of calculating comparable safety factors in all methods of analyses. Furthermore, analogous shear strain accumulation zones and shear strain values were found between the strength criteria using the FEM and FDM.
(5) Shear strain accumulation zones of the FDM depict recognisable failure modes correlating to those of the LEMs, while the FEM portrays widely distributed strains with slippage along joints.

This study shows the importance of performing more than one type of analyses in assessing slope stability, and the significance of identifying potential failure mechanisms from the conceptual to design level. The results of the current study also suggest that a less conservative design approach could be adopted based on the inclusion of rock bridges, through joint network simulations, which could potentially yield greater economic benefits.

Declaration of Competing Interest

The authors wish to confirm that there are no known conflicts of interest associated with this publication and there has been no significant financial support for this work that could have influenced its outcome.

Acknowledgements

The first author would like to acknowledge the Council of Geosciences for supporting her studies towards MSc completion. The authors would like to thank Consultant D for sharing the data and giving the opportunity to conduct this study. We also thank the editor and the two anonymous reviewers, whose suggestions have greatly improved the manuscript.

References

Amadei B, Savage WZ, Swolfs HS. Gravitational stresses in anisotropic rock masses. International Journal of Rock Mechanics and Mining Sciences and Geomechanics Abstracts 1987;24(1):5–14.
Barton NR. Predicting the behaviour of underground openings in rock. Norwegian Geotechnical Institution; 1987.
Barton NR. Review of a new shear strength criterion for rock joints. Engineering Geology 1973;7(4):287–332.
Barton NR. The shear strength of rock and rock joints. International Journal of Rock Mechanics and Mining Sciences and Geomechanics Abstracts 1976;13(9):255–79.
Belytschko T, Black T. Elastic crack growth in finite elements with minimal remeshing. International Journal of Numerical Methods in Engineering 1999;45(5):601–20.
Bieniawski ZT. Engineering rock mass classifications: a complete manual for engineers and geologists in mining, civil, and petroleum engineering. New York, USA: Wiley; 1989.
Bye AR, Bell FG. Stability assessment and slope design at Sandsloot open pit, South Africa. International Journal of Rock Mechanics and Mining Sciences 2001;38(3):449–66.
Call RD, Cicchini PF, Ryan TM, Barkley RC. Managing and analyzing overall pit slopes. In: Hustrulid WA, McCarter MK, Van Zyl DJA, editors. Slope stability in surface mining. Littleton, USA: Society for Mining, Metallurgy and Exploration; 2001. p. 39–46.
Consultant A. Consultant's report. Johannesburg, South Africa. 1996.
Consultant B. Feasibility study, section 4 – mining. Johannesburg, South Africa. 2006.
Consultant C. Review of pit slope design for north pit. Johannesburg, South Africa. 2009.
Consultant D. Rockfall hazard mitigation project. Report 13025-10512-1. Johannesburg, South Africa. 2011.
Cundall PA, Strack ODL. Discrete numerical model for granular assemblies. Geotechnique 1979;29(1):47–65.

Dershowitz W. Rock joint systems (PhD Thesis). Cambridge, USA: Massachusetts Institute of Technology; 1985.
Dershowitz WS, Einstein HH. Characterizing rock joint geometry with joint system models. Rock Mechanics and Rock Engineering 1988;21(1):21–51.
Dershowitz WS, Finnila A, Rogers S, Hamdi P, Moffitt KM. Step path rock bridge percentage for analysis of slope stability. In: 51st US Rock Mechanics/Geomechanics Symposium 2017. 5; 2017. p. 3650–8.
Eberhardt E, Stead D, Coggan JS. Numerical analysis of initiation and progressive failure in natural rock slopes – the 1991 Randa rockslide. International Journal of Rock Mechanics and Mining Sciences 2004;41(1):69–87.
Einstein HH, Veneziano D, Beacher GB, O'Reilly KJ. The effect of discontinuity persistence on rock slope stability. International Journal of Rock Mechanics and Mining Sciences and Geomechanics Abstracts 1983;20(5):227–36.
Einstein HH. Modern developments in discontinuity analysis: the persistence-connectivity problem. In: Hudson JA, editor. Comprehensive rock engineering. Principles – practice and projects. Volume 3: rock testing and site characterization. Pergamon Press; 1993. p. 193–213.
Elmo D, Clayton C, Rogers S, Beddoes R, Greer S. Numerical simulations of potential rock bridge failure within a naturally fractured rock mass. In: Proceedings of the 2011 international symposium on rock slope stability in open pit mining and Civil engineering. The South African Institute of Mining and Metallurgy; 2011.
Elmo D, Donati D, Stead D. Challenges in the characterisation of intact rock bridges in rock slopes. Engineering Geology 2018;245:81–96.
Fillion MH, Hadjigeorgiou J. Implications of collected additional data on the slope design in an open pit operation. Journal of the Southern African Institute of Mining and Metallurgy 2016;116(5):357–66.
Fisher R. Dispersion of a sphere. Proceedings of the Royal Society of London 1953;217(1130):295–305.
Goodman RE. Introduction to rock mechanics. 2nd ed. New York, USA: Wiley; 1989.
Hammah RE, Yacoub T, Curran JH. Variation of failure mechanisms of slopes in jointed rock masses with changing scale. In: Diederichs M, Grasselli G, editors. ROCKENG09: proceedings of the 3rd CANUS rock Mechanics symposium. Toronto, Canada; 2009.
Hoek E, Bray JW. Rock slope engineering. Revised 3rd ed. London, UK: The Institution of Mining and Metallurgy; 1981. p. 341–51.
Hoek E, Brown ET. Empirical strength criterion for rock masses. Journal of Geotechnical and Geoencironmental Engineering 1980;106(GT9):1013–35.
Hoek E, Brown ET. Practical estimates of rock mass. International Journal of Rock Mechanics and Mining Sciences 1997;34(8):1165–86.
Hoek E, Brown ET. The Hoek-Brown failure criterion – a 1988 update. In: Curran JC, editor. Proceedings of the 15th Canadian rock Mechanics symposium. Department of Civil Engineering, University of Toronto; 1988. p. 31–8.
Hoek E, Carranza-Torres C, Corkum B. Hoek-Brown failure criterion – 2002 edition. In: Proceedings of NARMS-TAC conference. Toronto, Canada; 2002. p. 273–367.
Hoek E. Practical rock engineering. Rocscience Inc.; 2007.
Hoek E. Putting numbers to geology – an engineer's viewpoint. Quarterly Journal of Engineering Geology and Hydrogeology 1999;32(1):1–19.
Itasca. Itasca software products – FLAC, FLAC3D, UDEC, 3DEC, PFC, PFC3D. Minneapolis, USA: Itasca Consulting Group Inc.; 2011.
Jakubec J, Terbrugge PJ, Guest AR, Ramsden F. Pit slope design at Orapa mine. In: Hustrulid WA, McCarter MK, Van Zyl DJA, editors. Slope stability in surface mining. Littleton, USA: Society for Mining, Metallurgy and Exploration; 2001. p. 227–38.
Jennings JE. A mathematical theory for the calculation of the stability of open cast mines. In: van Rensburg PWJ, editor. Planning open pit mines: Proceedings of the symposium on the theoretical background to the planning of open pit mines with special reference to slope stability. The South African Institute of Mining and Metallurgy/A.A. Balkema; 1970. p. 87–102.
Jimenez-Rodriguez R, Sitar N. Influence of stochastic discontinuity network parameters on the formation of removable blocks in rock slopes. Rock Mechanics and Rock Engineering 2008;41:563. https://doi.org/10.1007/s00603-006-0124-5.
Li G, Li H, Kato H, Mizuta Y. Application of ubiquitous joint model in numerical modelling of Hilltop Mines in Japan. Chinese Journal of Rock Mechanics and Engineering 2003;22(6):951–6.
Moes N, Dolbow J, Belytschko T. A finite element method for crack growth without remeshing. International Journal of Numerical Methods in Engineering 1999;46(1):131–50.
Moradi A, Hosseinitoudeshki V. The effect of joint models on the stability of rock slopes. International Journal of Geology, Agriculture and Environmental Sciences 2015;3(1):7–10.
Palisade. @Risk, risk analysis and simulation ad-in for microsoft excel. New York, USA: Palisade Corporation; 1997. http://www.palisade.com/risk/.
Read J, Stacey P. Guidelines for open pit slope design. CSIRO Publishing; 2009.
Riquelme A, Tomás R, Cano M, Pastor JL, Abellán A. Automatic mapping of discontinuity persistence on rock masses using 3D point clouds. Rock Mechanics and Rock Engineering 2018;51(10):3005–28.
Rocscience Inc. Rocscience software suite – RocData, dips, RocFall, swedge, RocPlane, RocTopple, slide, Phase2. Toronto, Canada: Rocscience Inc.; 2015.
Romer C, Ferentinou M. The significance of identifying potential failure mechanisms from conceptual to design level for open pit rock slopes. In: AfriRock 2017. The Southern African Institute of Mining and Metallurgy; 2017. p. 351–63.
Romer C. Rock slope stability analysis and rock fall hazard assessment in an open pit mine (MSc Thesis). University of KwaZulu-Natal; 2017.
Shang J, Hencher SR, West LJ, Handley K. Forensic excavation of rock masses: a technique to investigate discontinuity persistence. Rock Mechanics and Rock Engineering 2017;50(11):2911–28.
Shen B. Mechanics of fractures and intervening bridges in hard rocks (PhD Thesis). Stockholm, Sweden: Division of Engineering Geology, Royal Institute of Technology; 1993.
Shi GH, Goodman RE. Two-dimensional discontinuous deformation analysis. International Journal for Numerical and Analytical Methods in Geomechanics 1985;9(6):541–56.
Shi GH. Manifold method of material analysis. In: Transaction of the 9th army conference on applied mathematics and computing. Minneapolis, USA; 1991. p. 57–76.
Shi GH. Modeling rock joints and blocks by manifold method. In: Proceedings of the 33rd US symposium on rock Mechanics (USRMS). Rotterdam, The Netherlands: A.A. Balkema; 1992. p. 639–48.
Singh VK, Pradad M, Dhar BB. Stability analysis of an open pit mine by numerical modelling. Journal of Mines Metals and Fuels 1994;42:39–46.
Sjöberg J. Analysis of large scale slopes (PhD Thesis). Lueå, Sweden: Lueå University of Technology; 1999.
Sjöberg J. Failure Mechanisms for high slopes in hard rock. In: Hustrulid WA, McCarter MK, Van Zyl DJA, editors. Slope stability in surface mining. Littleton, USA: Society for Mining, Metallurgy and Exploration; 2001. p. 71–80.
Soren K, Budi G, Sen P. Stability analysis of open pit slope by finite difference method. International Journal of Research in Engineering and Technology 2014;3(5):326–34.
Stacey TR, Xianbin Y, Armstrong R, Keyter GJ. New slope stability considerations for deep open pit mines. Journal of the South African Institute of Mining and Metallurgy 2003;103(6):373–89.
Stead D, Eberhardt E, Coggan JS. Developments in the characterization of complex rock slope deformation and failure using numerical modelling techniques. Engineering Geology 2006;83(1–3):217–35.
Stead D, Eberhardt E. Understanding the mechanics of large landslides. In: Proceedings of international conference on vajont 1963–2013: thoughts and analyses after 50 Years since the catastrophic landslide. Padua, Italy; 2013.
Terzaghi K. Stability of steep slopes on hard unweathered rock. Geotechnique 1962;12(4):251–70.
Tuckey Z, Stead D. Improvements to field and remote sensing methods for mapping discontinuity persistence and intact rock bridges in rock slopes. Engineering Geology 2016;208:136–53.
Valdivia C, Lorig L. Slope stability at escondida mine. In: Hustrulid WA, McCarter MK, Van Zyl DJA, editors. Slope stability in surface mining. Littleton, USA: Society for Mining, Metallurgy and Exploration; 2001. p. 153–62.
Veneziano D. Probabilistic model of joints in rock. Cambridge, USA: Massachusetts Institute of Technology; 1978.
Walton S, Hassan O, Morgan K, Brown MR. Modified cuckoo search: a new gradient free optimisation algorithm. Chaos Solitons and Fractals 2011;44(9):710–8.
Wang T, Huang T. A constitutive model for the deformation of a rock mass containing sets of ubiquitous joints. International Journal of Rock Mechanics and Mining Sciences 2009;46(3):521–30.
Wen A, Sturzenegger M, Stead D. Analysis of a complex rock slope instability with a stepped failure surface using discrete fracture network models. In: Proceedings of the 1st international discrete fracture network engineering conference. Vancouver, Canada; 2014.
Wong LNY, Wu Z. Application of the numerical manifold method to model progressive failure in rock slopes. Engineering Fracture Mechanics 2014;119:1–20.
Zhang L. Engineering properties of rock. 2nd ed. Elsevier; 2016.
Zheng H, Liu DF, Li C. Slope stability analysis based on elasto-plastic finite element method. International Journal for Numerical Methods in Engineering 2005;64(14):1871–88.

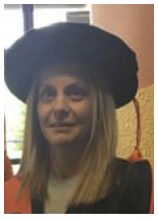

Dr. M. Ferentinou graduated with a degree in Geology from the University of Patras and a PhD degree in Engineering Geology from the National Technical University of Athens, where she has spent three years as post-doctor researcher. Her first academic employment was a lectureship in Engineering Geology at the Department of Civil and Construction Engineering at the Technological Educational Institute of Athens, followed by a lectureship in Engineering Geomorphology and Geographical Information systems at the Charokopio University of Athens. Ferentinou has been working in the industry in the consulting sector from 1997 to 2005, and was involved in more than 40 major infrastructure projects, such as the Athens Metro tunnel, and Egnatia Odos Project. She joined the University of Johannesburg in July 2016 and is currently an associate professor in Geotechnics - Engineering Geology. Ferentinou has authored and co-authored more than 50 papers published in peer-reviewed journals and international conference proceedings. She is a member of the Editorial Board of the journal *Bulletin of Engineering Geology and the Environment*. She is a member of the joint International Association of Engineering Geology (IAEG) commission C37 – on Landslides Nomenclature. She is rated by the National Research Foundation in South Africa as an established researcher (C2). Ferentinou's research focuses on landslide susceptibility assessment, slope stability, rock engineering systems, applications of artificial intelligence in geotechnics, and geographic information system (GIS) based applications in geohazard risk assessment. Currently she is engaged in the study of slope failure mechanism, and sinkhole propagation using fibre Bragg gratings and small-scale physical modelling.